Proceedings of the Estonian Academy of Sciences,
2016, **65**, 1, 28–36
doi: 10.3176/proc.2016.1.02
Available online at www.eap.ee/proceedings

ENGINEERING

Time-efficient automated analysis for fibre orientations in steel fibre reinforced concrete

Emiliano Pastorelli[a] and Heiko Herrmann[a,b*]

[a] Centre for Nonlinear Studies, Institute of Cybernetics at Tallinn University of Technology, Akadeemia tee 21, 12618 Tallinn, Estonia
[b] Institut für Physik, Technische Universität Chemnitz, Chemnitz, Germany

Received 1 April 2015, accepted 30 April 2015, available online 10 December 2015

Abstract. One of the most important factors to determine the mechanical properties of a fibre composite material is the orientation of the fibres in the matrix. Their orientation might differ in distinct parts of the structural element as dependent on the casting techniques and mould materials. This paper presents an algorithm to retrieve information on a single fibre's orientation out of SFRC samples scanned through a μCT scanner. The software implemented with the algorithm includes a data filtering component to remove the noise from the data sets and prepare them correctly for analysis. Due to its short computational times and its almost complete lack of need for external user intervention, the software is able to process and analyse large batches of data in short periods by providing results in a variety of visual and numerical formats.

Key words: computer engineering, image analysis, tomography, steel fibre reinforced concrete, fibre orientation.

1. INTRODUCTION

Steel Fibre Reinforced Concrete (SFRC) is a cementitious composite material made of cement and aggregate, which incorporates discrete discontinuous fibres. Thanks to its advantages in terms of production speed and required labour force, SFRC is probably going to gradually supplement or substitute the traditional concrete reinforced with metal bars or grids in several construction industry applications.

The need to reinforce concrete arises from the nature of the material itself. Unreinforced concrete is brittle and with a low tensile strength and low strain capacity. In order to perform properly and to prevent sudden failure, it needs bridging the microcracks that propagate in its structure. In the specific case of SFRC described in this paper, this is achieved by incorporating into the mixture a certain amount of steel fibres with hooked ends, 50 mm long and 1 mm thick. Their presence is fundamental in order to improve the mechanical property of the material. They help the concrete in bearing part of the tensile stress and chemically and mechanically transfer the remaining part to more stable regions of the matrix. Multiple factors influence the efficiency of the fibres: shape, volume fraction, aspect ratio, their surface properties, and their orientation [1,2].

As the orientation distribution of the fibres within the matrix is non-uniform, the properties of the system often tend towards anisotropy [3,4]. A number of investigations [5–9] demonstrated the strong influence that the orientation has on the material properties.

* Corresponding author, hh@cens.ioc.ee

2. MOTIVATION OF THE RESEARCH

Several methods already exist in order to extract orientation information from X-ray tomographies of SFRC concrete [10–13]. Most of them are based on approaches very different from one another, among which are skeletonization [10], linear regression [12], and separate regions labelling [13]. For several of them though, the use of commercial software and libraries prevented the disclosure of the detailed implementation of the methods. Additionally, most of the methods require either long processing times or user interaction along the process or even both. This prevents the overnight processing of large batches of data sets, slowing down the whole research process and increasing the possibility for mistakes.

In order to find a solution to the above-mentioned problems, we decided to design and implement our own algorithm. The choice was made bearing in mind the need to have a flexible fast system for the analysis that could be progressively expanded and improved according to new needs that might arise during our research.

3. INTRODUCTION TO THE ANALYSIS

The development of the algorithm was initially inspired by Redenbach et al. [14] and by their use of the Hessian matrix to detect cylindrical shapes in the volumes. However, its pure application, developed for higher density straight fibres, could not perform correctly in order to analyse the sparsely distributed hooked-end fibres of our samples. Our specific data sets provided moreover a variety of additional challenges that required a more complex combined approach.

The first step of the process was to filter them in order to optimize the data to be fed to the analysis. Filtering was done with the Insight Toolkit (ITK) libraries [15] in order to flag on the volume all the voxels that would not be of interest for the analysis. This meant for the analysis to ignore all the voxels belonging to the matrix (cement, aggregate, and air bubbles), all the scanning artefacts, and noise.

In better formed data sets (i.e. with no touching fibres), this phase might also be sufficient to already isolate and label each fibre separately. Unfortunately, it was not the case for our data. Due to the tomographic reconstruction and partly as a by-product of the data filtering to isolate cylindrical shapes with the Frangi Vesselness filter [16], it is very rare to have completely separated fibres. Most of them have indeed contact points with other fibres, quite often forming chains of fibres of three or more elements. Only two input parameters are needed in order to perform data filtering: the thickness of the fibres (in voxels) and the threshold for binarization. The former depends on the properties of the specific type of SFRC analysed and the scanner resolution. The latter depends on the properties of the scanner and of the analysed material and the volume reconstruction. Both parameters remain constant for all the samples belonging to a batch of the same material scanned with the same technique and devices and using the same parameters for the volume reconstruction.

4. ANALYSIS

The data prepared for the analysis after the filtering phase was
- cleared of all the voxels not belonging to fibres,
- binarized,
- the non-touching regions were labelled uniquely [17] and their indices were stored to a file, and
- the data was smoothed with a Gaussian 3D filter.

The last step, in particular, was necessary in order to use the Hessian-based method mentioned in the previous section.

The Hessian matrix is the square matrix of the second-order partial derivatives of a function. When such a matrix is calculated for each pixel/voxel of a greyscale image (be it 2- or 3-dimensional), its eigenvalues and eigenvectors contain an important set of information about the input element: the variation of intensity

of the grey level in all the directions. Equations (1)–(4) and Fig. 1 show the construction of the matrix on a 2D image:

$$(H)_{ij} = \left(\frac{\partial^2 f}{\partial i \partial j}\right), \text{ where } i,j = x,y, \tag{1}$$

$$\frac{\partial^2 f(x,y)}{\partial x \partial x} \approx \frac{f(x+1,y)-2f(x,y)+f(x-1,y)}{h^2}, \tag{2}$$

$$\frac{\partial^2 f(x,y)}{\partial y \partial y} \approx \frac{f(x,y+1)-2f(x,y)+f(x,y-1)}{k^2}, \tag{3}$$

$$\frac{\partial^2 f(x,y)}{\partial x \partial y} \approx \frac{f(x+1,y+1)-f(x+1,y-1)-f(x-1,y+1)+f(x-1,y-1)}{4hk}, \tag{4}$$

here h and k are the pixel (voxel) sizes in x and y directions. In 3D, $i,j = x,y,z$ and corresponding equations for z would be added. In order to be constructed correctly, the matrix requires the cylindrical elements to have a grey level gradient from the inside (high values) to the outside (lower values).

A problem related to our specific data sets arose from the scanning devices not being prepared to process so large concrete samples (10 cm in diameter). Because of that, the reconstructed volumes presented a cylindrically shaped artefact (see Fig. 2) in their centre. This artefact contaminated the analysis for multiple reasons. It connected multiple touching fibres regions, making their subsequent separation even more complex, but it also could have been recognized by the analysis as a very large fibre (due to the cylindrical shape), and would have been therefore difficult to manage in the automated analysis.

In order to avoid problems, we filtered the data prior the analysis by coring out the voxels belonging to a parallelepiped-shaped region wrapping the artefact. The results with the core removed immediately proved to be much better than the ones with it still in the volume.

For each voxel belonging to a fibre (using the labels stored during the filtering) the algorithm calculates the Hessian matrix and extracts its eigenvectors. The smallest of them represents the direction of the fibre in that specific voxel (Fig. 1). The orientation vectors for each of the regions are then stored together for

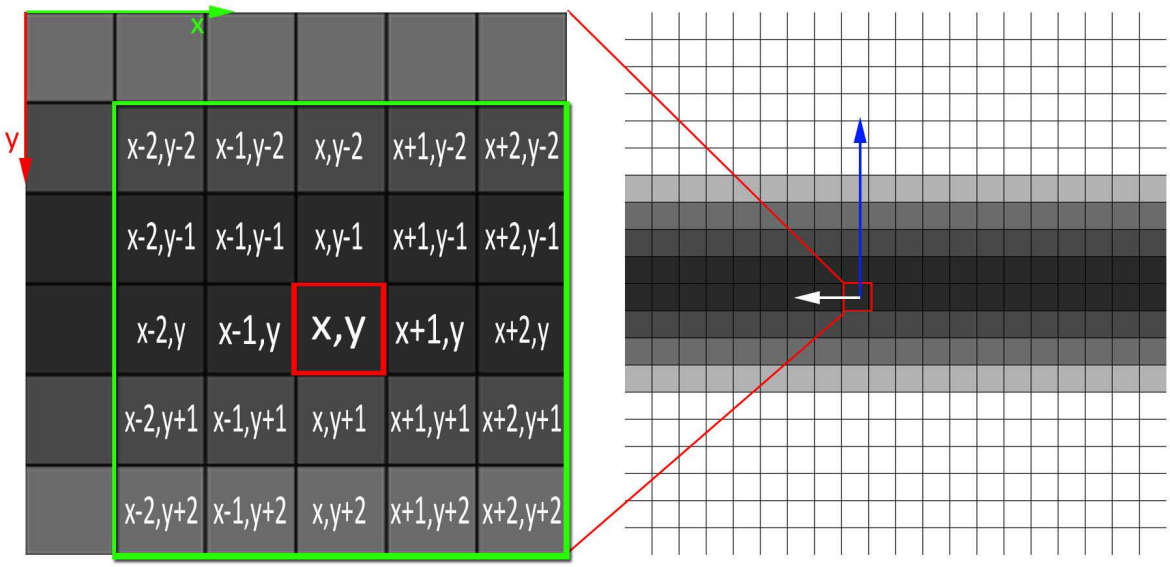

Fig. 1. Pixels used for the construction of the 2D greyscale-based Hessian matrix. The direction of the eigenvectors of the matrix in one point is also indicated.

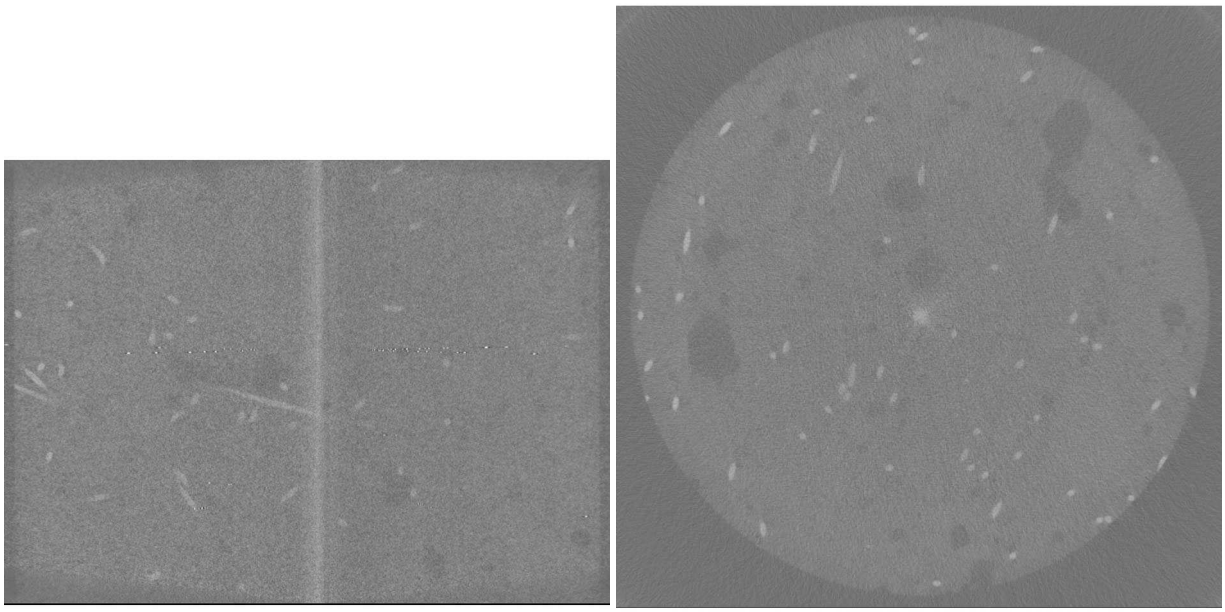

Fig. 2. Slice images of the tomography showing the artefact in the middle.

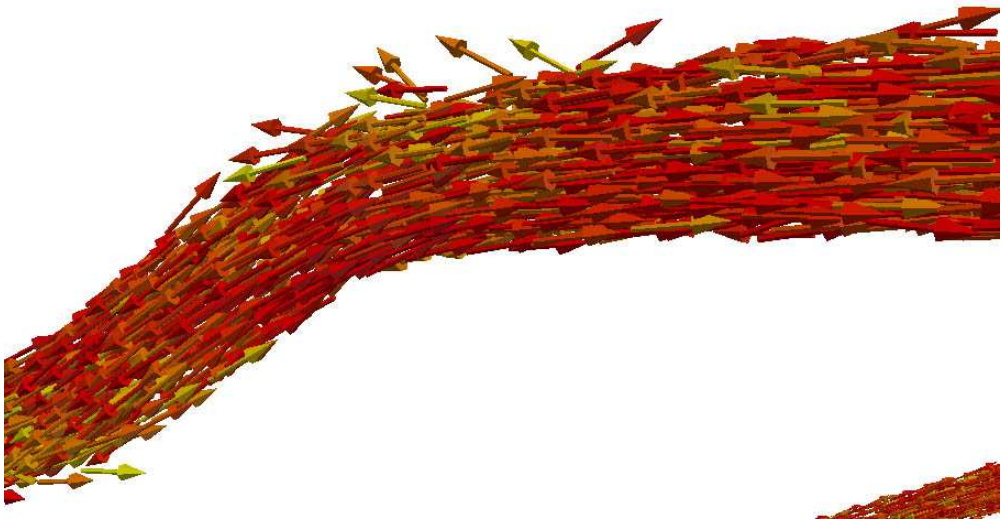

Fig. 3. Detail on the voxel vectors in the proximity of one of the hooked ends of a fibre.

the next phase of the analysis. The data gathered so far though do not represent the fibres' main shaft contribution (i.e. the important one to determine the fibres' contribution at crack time) due to the presence of those vectors that belong to the hooked ends (Fig. 3). In the next section we explain the algorithm we developed to extract the main orientation of the fibres.

5. SEPARATION OF TOUCHING FIBRES

The next step was the most important one of the algorithm in order to identify the orientation of the single fibres. The idea came from the observation of the voxel vectors visualized on the Kyb3 system, our Virtual Reality environment [18]. Even in the case of chains of touching fibres it was quite obvious from the visual inspection that the majority of orientation vectors were aligned along the shafts of the fibres. Therefore the distribution of the orientation vectors of the voxels should show peaks corresponding to the main shafts of each fibre. Unless two fibres of the chain had an identical orientation (in which case they would be seen as a single very large peak), this behaviour had to be isolated and analysed properly.

To cast the data into a more easily analysable format, we converted the voxel orientation vectors from cartesian to spherical coordinates. This operation suffers some of the weaknesses of the spherical coordinates for angles very close to the poles of the sphere, but allows clustering to be done more easily on a 90×360 2D matrix. As the indices of the matrix we used the ϑ angle to represent the rotation on the z axis (polar angle) and the φ angle for the rotation on the x–y-plane (azimuthal angle). In order to clean the results from noise and facilitate peak detection, we smoothed the whole matrix with a simple Gaussian filtering.

The analysis of a single fibre (a rare occurrence in the data set) generates a single dominating peak and represents no particular problem for the detection (Fig. 4a). The case of multiple touching fibres was slightly more complex (Fig. 4c). The angles corresponding to the main fibres orientation, though, generated peaks of a size easily identifiable in the matrix (Fig. 4b). To ignore the noise and the much

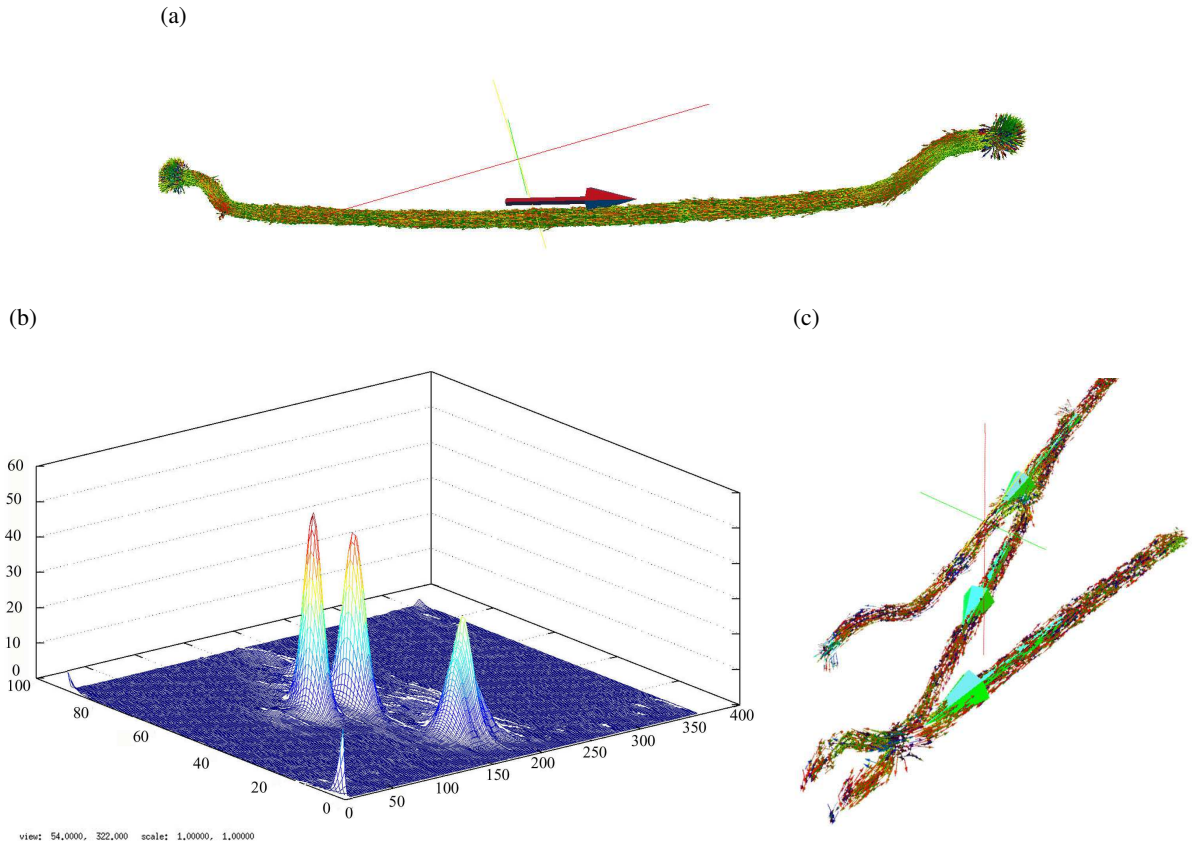

Fig. 4. A single fibre orientation extraction (a), the peaks describing three touching fibres (b), and the three touching fibres separate orientations after the analysis of the region's peaks map (c).

smaller peaks resulting from the hooked ends of the fibre, we thresholded the data proportionally to the highest peaks in the matrix. We then proceeded to isolate the separate clusters through a connected regions labelling algorithm [19]. In each of the clusters, we proceeded then by locating the highest local peak, i.e. the one corresponding to the fibre shaft orientation.

As the last step we converted back the angles from spherical to cartesian coordinates. The outcome was that we now had the centre point (obtained by averaging the coordinates of all the voxels belonging to the peak) and the orientation for each fibre.

6. PERFORMANCES AND TIMINGS

While the filtering process can be expensive in terms of resources (the ITK Frangi Vesselness filter [20] applied to a $900 \times 900 \times 576$ volume requires up to 32GB of RAM) and takes approximately 23 to 25 min per volume, the analysis component of the software is, by contrast, very fast and lightweight. Thanks to the labels provided by the filtering phase, only the relevant voxels are analysed while all the others are completely skipped, which speeds computation up additionally.

A series of optimization in the use of the data structure allows running the whole process on a $900 \times 900 \times 576$ data set in a time that ranges between 2 and 3.5 min depending on the amount of fibres in the volume. The RAM consumption for the analysis barely reaches 4GB and requires absolutely no additional input from the user. The whole filtering and analysis process for a single data set can be therefore performed in approximately 25 to 28 min.

7. VALIDATION OF RESULTS

The validation of the algorithm and its implementation were made in two ways: visually and numerically. The visual feedback was used throughout the whole development for a quick testing of the correctness of all the steps (Fig. 4) from filtering until the final analysis.

Throughout software execution, we saved a variety of data describing each step's outcome in formats easy to read and visualize. This allowed a constant correctness control and the possibility of quickly detecting and correcting algorithmic and implementation mistakes. The data produced at the end of the whole analysis consisted of

- a volume file (in the NRRD/NHDR format [21]; header + raw volume) containing the filtered and smoothed volume showing only the fibres,
- a VTK [22] point based visualization file containing all the voxel vectors of all fibres (Fig. 5),
- a VTK file containing the single fibre orientation vectors correctly positioned in space.

As it can be seen in Figs 3, 4, and 5, the voxel vectors and fibre orientation vectors show unambiguously the correctness of the algorithm and the software.

In order to perform a numerical validation, we compared the results of the analysis with those provided by the skeletonization approach [10] on the same data sets. Aside from small differences depending on a variety of factors, the two analyses were very similar in the results. The scatterplots in Fig. 6 show the superposition of the fibre orientation angles as obtained by skeletonization (Fig. 6a) and by our method (Fig. 6b). The comparison performed correctly on all the 15 data sets. By using the same equations described in [8,10,23], we calculated from the data the order parameter and director describing the orientation of the fibres in the sample.

The director is the eigenvector corresponding to the largest eigenvalue (according to absolute value: $|\lambda_1| \geq |\lambda_2| \geq |\lambda_3|$) of the second order alignment tensor $\mathbf{A}$ that is described as

$$\mathbf{A} = \frac{1}{N} \sum_{i=1}^{N} \overline{\mathbf{n}_i \otimes \mathbf{n}_i}, \tag{5}$$

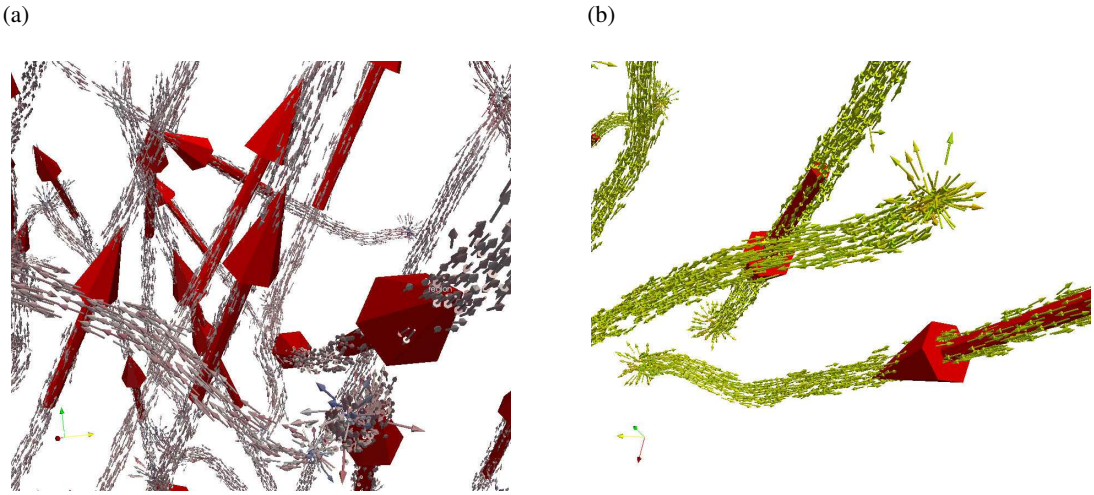

Fig. 5. Full orientation extraction, voxel, and fibres vectors (a) and orientation extraction detail on a single fibre (b).

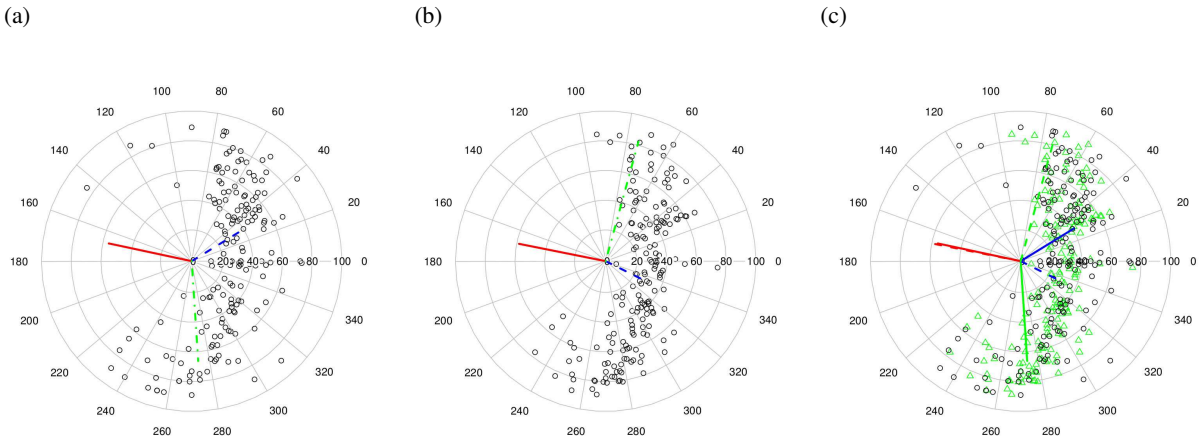

Fig. 6. Scatterplot describing the orientation angles in a sample: (a) with the skeletonization method [10], (b) with the method described in this paper, and (c) the superposition of the two results.

where $\mathbf{n}_i$ represents the direction of the i-th fibre, N is the total amount of fibres, and $\overline{\mathbf{n}_i \otimes \mathbf{n}_i}$ is the symmetric traceless tensor product. The order parameter is given as

$$S = \frac{3}{2}\lambda_1 \tag{6}$$

or as

$$S = \left\langle \frac{3}{2}\cos^2\alpha - \frac{1}{2} \right\rangle \tag{7}$$

with λ_1 the largest eigenvalue of $\mathbf{A}$ and α the angle between the individual fibre and the director.

The director of the sample displayed in Fig. 6 (expressed in ϑ and φ angles) is $(\varphi = 169, \vartheta = 59)$ for the skeletonization approach and $(\varphi = 168, \vartheta = 57)$ with our method. The order parameter $S = -0.44$ for the skeletonization and $S = -0.41$ for our algorithm. The differences between the parameters are sufficiently small to validate the results.

8. CONCLUSION

Although still under improvement, the described method and software already proved to provide very reliable results. The limited human interaction and very fast processing times minimize the possibility for human errors and allow autonomous analysis of large batches of data.

The software builds its own structured directories in order to store all the output orderly and process the numeric data further for additional analyses. With further steps towards an even more precise analysis of the peaks in order to succeed also in case of very similarly aligned fibres and a more easily usable graphical interface, we strongly believe that the software has a chance to become a widespread tool for SFRC analysis.

ACKNOWLEDGEMENTS

This research was supported by the European Union through the European Regional Development Fund, in particular through funding for the Centre for Nonlinear Studies as an Estonian national centre of excellence. It was compiled with the assistance of the Tiger University Program of the Estonian Information Technology Foundation (VisPar/Kyb3 visualization system, EITSA/HITSA grants 10-03-00-24, 12-03-00-11, and 13030009). This research was supported by European Social Fund's Doctoral Studies and Internationalisation Programme DoRa T4, which is carried out by the Archimedes Foundation (scholarship for E.P.). E.P. also gratefully acknowledges the ICT doctoral school for the study grant for the academic year 2014/2015.

REFERENCES

1. Bentur, A. and Mindess, S. *Fibre Reinforced Cementitious Composites*. Taylor & Francis, London and New York, 2007.
2. Tejchman, J. and Kozicki, J. *Experimental and Theoretical Investigations of Steel-fibrous Concrete*. 1st ed. Springer Series in Geomechanics and Geoengineering. Springer, 2010.
3. Eik, M., Lõhmus, K., Tigasson, M., Listak, M., Puttonen, J., and Herrmann, H. DC-conductivity testing combined with photometry for measuring fibre orientations in SFRC. *J. Mater. Sci.*, 2013, **48**(10), 3745–3759.
4. Eik, M. and Herrmann, H. Raytraced images for testing the reconstruction of fibre orientation distributions. *Proc. Estonian Acad. Sci.*, 2012, **61**, 128–136.
5. Grünewald, S., Laranjeira, F., Walraven, J. C., Aguado, A., and Molins, C. Influence of fibre orientation on the performance of steel fibre-reinforced concrete. In *8th RILEM International Symposium on Fiber Reinforced Concrete: Challenges and Opportunities (BEFIB 2012)*. Rilem Publications SARL, 2013, 313–325.
6. Wuest, J., Denarie, E., Bruhwiler, E., Tamarit, L., Kocher, M., and Gallucci, E. Tomography analysis of fiber distribution and orientation in ultra high-performance fiber-reinforced composites with high-fiber dosages. *Exp. Techniques*, 2009, **33**(5), 50–55.
7. Le, T. H., Dumont, P. J. J., Orgeas, L., Favier, D., Salvo, L., and Boller, E. X-ray phase contrast microtomography for the analysis of the fibrous microstructure of SMC composites. *Composites Part A: Appl. Sci. Manuf.*, 2008, **39**(1), 91–103.
8. Herrmann, H., Eik, M., Berg, V., and Puttonen, J. Phenomenological and numerical modelling of short fibre reinforced cementitious composites. *Meccanica*, 2014, **49**(8), 1985–2000.
9. Eik, M., Puttonen, J., and Herrmann, H. An orthotropic material model for steel fibre reinforced concrete based on the orientation distribution of fibres. *Compos. Struct.*, 2015, **121**, 324–336.
10. Suuronen, J. P., Kallonen, A., Eik, M., Puttonen, J., Serimaa, R., and Herrmann, H. Analysis of short fibres orientation in Steel Fibre Reinforced Concrete (SFRC) using X-ray tomography. *J. Mater. Sci.*, 2013, **48**(3), 1358–1367.
11. Schnell, J., Schladitz, K., and Schuler, F. Richtungsanalyse von Fasern in Betonen auf Basis der Computer-Tomographie. *Beton- und Stahlbetonbau*, 2010, **105**(2), 72–77.
12. Vicente, M. A., Gonzalez, D. C., and Minguez, J. Determination of dominant fibre orientations in fibre-reinforced high-strength concrete elements based on computed tomography scans. *Nondestructive Testing and Evaluation*, 2014, **29**(2), 164–182.
13. Ponikiewski, T., Katzer, J., Bugdol, M., and Rudzki, M. Steel fibre spacing in self-compacting concrete precast walls by X-ray computed tomography. *Mater. Struct.*, 2014, doi: 10.1617/s11527-014-0444-y.
14. Redenbach, C., Rack, A., Schladitz, K., Wirjadic, O., and Godehardt, M. Beyond imaging: on the quantitative analysis of tomographic volume data. *Int. J. Mater. Res.*, 2012, **103**(2), 217–227.
15. Johnson, H. J., McCormick, M., Ibáñez, L., and the Insight Software Consortium. The ITK Software Guide. Updated for ITK version 4.8. http://www.itk.org/ItkSoftwareGuide.pdf (accessed 26.10.2015).

16. Frangi, A. F., Niessen, W. J., Nederkoorn, P. J., Bakker, J., Mali, W. P. T. M., and Viergever, M. A. Quantitative analysis of vascular morphology from 3D MR angiograms: in vitro and in vivo results. *Magnet. Reson. Med.*, 2001, **45**, 311–322.
17. Lehmann, G. Label object representation and manipulation with ITK. 2007. http://hdl.handle.net/1926/584 (accessed 30.04.2015).
18. Pastorelli, E. and Herrmann, H. A small-scale, low-budget semi-immersive Virtual Environment for Scientific Visualization and Research. *Procedia Computer Science*, 2013, **25**(iii–iv), 14–22.
19. Dillencourt, M. B., Samet, H., and Tamminen, M. A general approach to connected-component labeling for arbitrary image representations. *J. ACM*, 1992, **39**(2), 253–280. http://doi.acm.org/10.1145/128749.128750 (accessed 30.04.2015).
20. Kroon, D. J. Hessian based Frangi Vesselness filter. 2010. http://www.mathworks.com/matlabcentral/fileexchange/24409-hessian-based-frangi-vesselness-filter (accessed 30.04.2015).
21. Kindlmann, G., Bigler, J., and Van Uitert, D. NRRD file format. 2008. http://teem.sourceforge.net/nrrd/format.html (accessed 30.04.2015).
22. Schroeder, W., Martin, K. M., and Lorensen, W. E. *The Visualization Toolkit (2nd ed.): An Object-oriented Approach to 3D Graphics*. Prentice-Hall, Inc., Upper Saddle River, NJ, USA, 1998.
23. Herrmann, H. and Eik, M. Some comments on the theory of short fibre reinforced material. *Proc. Estonian Acad. Sci.*, 2011, **60**, 179–183.

Efektiivne automatiseeritud meetod kiudude orientatsiooni määramiseks teraskiudarmeeritud betoonis

Emiliano Pastorelli ja Heiko Herrmann

Kiudude orientatsioon kiudarmeeritud materjalides sõltub suurel määral valmistamise tehnoloogiast ja mõjutab oluliselt materjali tugevusomadusi. Käesolevas artiklis on esitatud algoritm kiudude orientatsiooni määramiseks katsekehade skaneeritud mõõtetulemuste põhjal, mis võimaldab leida kiudude rivistustensorid. Nende teadmine võimaldab omakorda täpsustada materjali olekuvõrrandeid (pinge-deformatsioonivahelisi seoseid). Andmete visualiseerimiseks on konstrueeritud originaalne seade Kyb3 koos vastava tarkvaraga andmete edasiseks töötlemiseks, kasutades filtreid võimaliku müra eemaldamiseks. Tulemused on otseselt kasutatavad kiudarmeeritud materjalide tugevusanalüüsis.